J. Wind Eng. Ind. Aerodyn. 155 (2016) 1–10

Contents lists available at ScienceDirect

Journal of Wind Engineering and Industrial Aerodynamics

journal homepage: www.elsevier.com/locate/jweia

Aerodynamic benefit for a cyclist by a following motorcycle

Bert Blocken [a,b,*], Yasin Toparlar [a], Thomas Andrianne [c]

[a] Department of the Built Environment, Eindhoven University of Technology, P.O. Box 513, 5600 Eindhoven, The Netherlands
[b] Department of Civil Engineering, KU Leuven, Kasteelpark Arenberg 40 – Bus 2447, 3001 Leuven, Belgium
[c] Department of Aerospace and Mechanical Engineering, University of Liège, Allée de la Découverte, 9 Quartier Polytech 1, B52/3, B-4000 Liège, Belgium

ARTICLE INFO

Article history:
Received 23 April 2016
Received in revised form
27 April 2016
Accepted 27 April 2016

Keywords:
Computational Fluid Dynamics
Wind tunnel
Aerodynamic cyclist drag
Cycling aerodynamics
Following motor
Motorbike
Numerical simulation

ABSTRACT

In recent years, many accidents have occurred between cyclists and in-race motorcycles, even yielding fatal injuries. The accidents and the potential aerodynamics issues have impelled the present authors to perform dedicated wind-tunnel measurements and Computational Fluid Dynamics (CFD) simulations to assess cyclist drag reduction when followed by one, two or three motorcycles. The 3D steady-state Reynolds-Averaged Navier–Stokes simulations with the standard k–ε model are validated by the wind-tunnel tests. The cyclist drag reduction goes up to 8.7% for a single trailing motorcycle and to 13.9% for three trailing motorcycles at a distance of 0.25 m behind the cyclist. This distance is not uncommon in elite races, as evidenced by the many recent accidents. The effect by a single following motorcycle at realistic short distances d=0.25 m (8.7%), d=0.5 m (6.4%) and d=1 m (3.8%) is larger than that by a following car at realistic short distance d=5 m (1.4%). Therefore it could be argued that in-race motorcycles are not only more dangerous but also aerodynamically more influential. This study reinforces the necessity for the International Cycling Union to change the rules concerning in-race motorcycles, not only to avoid accidents but also to avoid unwanted aerodynamic benefits.

1. Introduction

It is well-known that the greatest potential for improvement in cycling speed is situated in its aerodynamics (Wilson, 2004). At racing speeds (about 54 km/h or 15 m/s in time trials), the aerodynamic resistance or drag is about 90% of the total resistance (Kyle and Burke, 1984, Grappe et al., 1997, Lukes et al., 2005). Aerodynamic drag can be assessed by field tests, wind-tunnel measurements and numerical simulation by Computational Fluid Dynamics (CFD). The use of CFD in wind engineering, also referred to as Computational Wind Engineering, has seen a rapid growth in the past 50 years (Murakami, 1997, Stathopoulos, 1997, Baker, 2007, Solari, 2007, Meroney and Derickson, 2014, Blocken, 2014, 2015). Indeed, also in cycling aerodynamics, several publications have reported CFD simulations (e.g. Hanna, 2002, Lukes et al., 2004, Defraeye et al., 2010a, 2010b, 2011, 2014, Blocken et al., 2013, Blocken and Toparlar, 2015, Fintelman et al., 2015). While most aerodynamic studies in cycling focused on the drag of a single (isolated) cyclist, several efforts have also been made to assess the effects of "drafting" (Kyle, 1979, McCole et al., 1990, Hagberg and McCole, 1990, Zdravkovich et al., 1996, Olds, 1998, Broker et al., 1999, Edwards and Byrnes, 2007, Iniguez-de-la-Torre and Iniguez, 2009, Blocken et al., 2013, Defraeye et al., 2014, Barry et al., 2015). Blocken et al. (2013) for the first time reported the aerodynamic effect for a leading cyclist due to a trailing cyclist based on CFD simulations and wind-tunnel measurements. Combining CFD simulations and wind-tunnel testing is clearly advocated in wind engineering for its synergistic effect (Meroney, 2016). Later, Blocken and Toparlar (2015) assessed the aerodynamic benefit for a cyclist by a trailing car, again by the combination of CFD simulations and wind-tunnel tests. This effect is not taken into account in elite cycling, as for individual time trials, the rules of the International Cycling Union UCI only specify a minimum distance between rider and car of 10 m because of safety reasons (International Cycling Union, 2015a, 2016). Furthermore, during actual races, this limit is often not kept because it is not strictly enforced. Nevertheless, during individual time trials, there is always at least one, but often more following cars, potentially influencing the drag of the cyclist (Fig. 1a, b and d). As a result, Blocken and Toparlar (2015) advised the UCI to modify their regulations for time trials and to fix the minimum distance for trailing cars at least at 30 m, which will not only avoid unwanted aerodynamic effects, but will also avoid dangerous situations for the riders. Indeed, the stopping distance of a car at 54 km/h on a wet road is much larger than 10 m.

Apart from cars, cycling races also contain a multitude of motorcycles, which can be neutral support motor cycles, commissaire

* Corresponding author at: Building Physics and Services, Eindhoven University of Technology, P.O. Box 513, 5600 MB Eindhoven, The Netherlands.
Tel.: +31 40 247 2138; fax +31 40 243 8595.
E-mail address: b.j.e.blocken@tue.nl (B. Blocken).

http://dx.doi.org/10.1016/j.jweia.2016.04.008

Fig. 1. Photographs from individual time trials: cyclist followed by motorcycle and/or car(s) (sources: a–d: International Cycling Union 2013, 2014, 2015b; e: www.zimbio.com; f: cyclingweekly.co.uk (Sunada); g: cyclingweekly.co.uk; h: www.hln.be).

Table 1
Non-exhaustive overview of motorcycle-cyclist crashes in the past two years in inverse chronological order.

Date	Race	Rider	Motorcycle	Consequences
2016/04/10	Paris-Roubaix (France)	Elia Viviani (Italy)	/	Chest trauma and cuts
2016/03/27	Gent-Wevelgem (Belgium)	Antoine Demoitié (Belgium)	Commissaire motorcycle	Rider deceased
2016/02/28	Kuurne-Brussel-Kuurne (Belgium)	Stig Broeckx (Belgium)	Medical motorcycle	Fractured collarbone and one rib, hand bruised, race lost
2015/09/02	Vuelta a Espana (Spain)	Sergio Paulinho (Portugal)	TV motorcycle	Race lost, abandoned tour
2015/08/29	Vuelta a Espana (Spain)	Peter Sagan (Slovakia)	Neutral support motorcycle	Race lost
2015/08/01	Clasica San Sebastian (Spain)	Greg Van Avermaet (Belgium)	TV motorcycle	Broken frame and back wheel, race lost
2015/07/23	Tour de France (France)	Jacob Fuglsang (Denmark)	Photographer motorcycle	Race lost.
2014/05/26	National championship (US)	Taylor Phinney (US)	/	Fractured leg, race lost
2014/05/26	National championship (US)	Lucas Euser (US)	/	Rear wheel and pedal broken, race lost

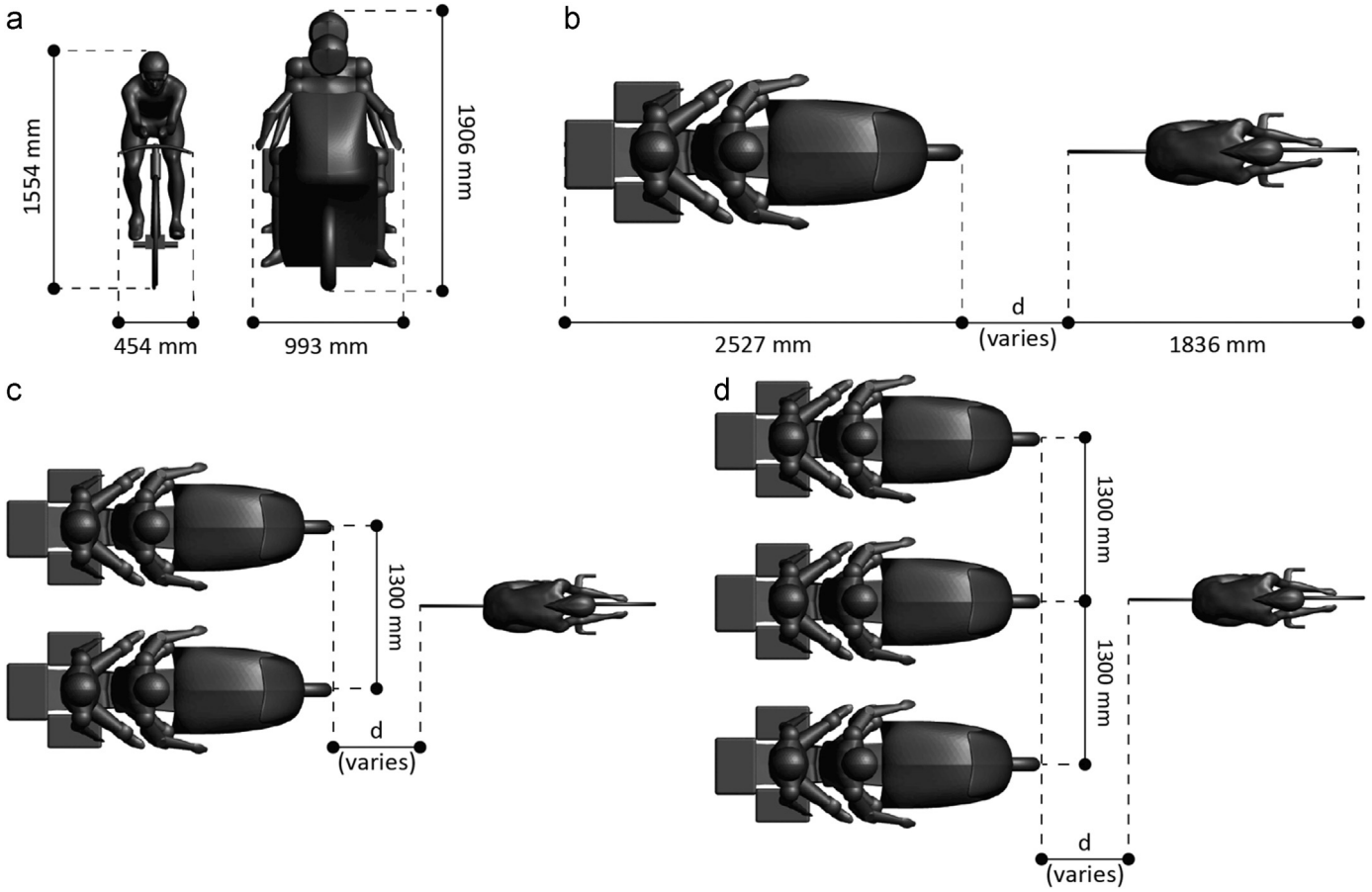

Fig. 2. Geometry of cyclist and motorcycle(s).

motorcycles, traffic manager motorcycles, information motorcycles, doctor and police motorcycles or press motorcycles, where the latter can be camera motorcycles, sound motorcycles or photographer's motorcycles. The press motorcycles are allowed to manoeuvre in the proximity of the cyclists when their passengers are filming or recording and filming is only forbidden in the last 500 m of the race (International Cycling Union, 2016). For individual time trials, following vehicles (which can be cars or motorcycles) are requested to follow at least 10 m behind the riders (International Cycling Union, 2016). However, this rule is not strictly enforced and especially press motorcycles ride often much closer to the cyclists. Fig. 1 shows some images of individual time trials with riders followed by motorcycles and/or cars.

The importance of motorcycles in races is exacerbated by the many accidents in recent years caused by motorcyclist-cyclist crashes, sometimes yielding severe injuries and even fatal injuries as in the Gent-Wevelgem race in Belgium in March 2016. Table 1 provides a non-exhaustive overview of crashes in the past two years in inverse chronological order. The aerodynamics issues and the many accidents have impelled the present authors to develop the research reported in this paper. We have performed dedicated wind-tunnel measurements and CFD simulations to assess the drag reduction for a cyclist when followed by one, two or three motorcycles. It should be noted that a cyclist followed by three vehicles is not uncommon for the top riders in time trials. As an example, Fig. 1h shows rider Laurent Fignon who was followed by 6 motorcycles in the final time trial in the legendary Tour de France of 1989, although this particular figure only shows 4 of the 6 motorcycles.

The paper is structured as follows. Section 2 reports the set-up of the wind-tunnel experiments. Section 3 contains the computational settings and parameters of the CFD simulations. Section 4 presents the results of the CFD simulations. In Section 5, the potential impact of the aerodynamic benefits addressed in Section 4 on the outcome

of individual time trial races is assessed. Finally, Section 6 (discussion) and 7 (conclusions) conclude the paper.

2. Wind tunnel experiments for cyclist and following motorcycle

The full-scale geometry and dimensions of cyclist and following motorcycle are given in Fig. 2. The height and the weight of the cyclist were 183 cm and 72 kg, respectively. He is equipped with an aerodynamic helmet and a standard tight-fitting racing suit with long sleeves. In time-trial position, the frontal area is 0.34 m². The bicycle is a standard racing bicycle with open wheel at the front and disk wheel at the rear and a time-trial handlebar. Both wheels are fixed. The wind-tunnel measurements were performed in the aeronautical section of the Wind Tunnel Laboratory at the University of Liège in Belgium. The cross-section of the test section is W x H = 2 × 1.5 m². A dedicated set-up with an elevated sharp-edge horizontal plate and embedded force balance was developed to limit boundary layer development (Fig. 3). To fully accommodate the models in the wind tunnel at a blockage ratio below 5%, they were manufactured at scale ¼, yielding a blockage ratio below 3.5%. Fig. 4 shows the models in the wind tunnel. Tests were performed at 60 m/s to ensure Reynolds number similarity with the (full-scale) CFD simulations and with reality at 15 m/s cycling speed, which is a typical elite time trial speed. Separation distances d=0.25, 0.5, 1, 1.5, 2, 2.5 m were considered. Drag in cycling is often quantified by the drag area AC_D (m²), which is the product of the frontal area of the cyclist (A) and the drag coefficient (C_D). It relates the drag force (F_D) to the dynamic pressure ($\rho U_\infty^2/2$):

$$F_D = AC_D \frac{\rho U_\infty^2}{2} \quad (1)$$

where ρ is the density of air (kg/m^3) and U_∞ the approach-flow air speed (m/s). The drag force, i.e. the horizontal component parallel to the wind direction and bicycle, was measured using a force transducer with a conservative maximum error estimate of 1.24 N with 95% confidence level, although the actual precision is expected to be much better (Gore 2016). It should be noted that this error includes both systematic and random errors, and that systematic errors were removed by biasing prior to every measurement. The data were sampled at 10 Hz for 180 s. During the measurements, air temperature and speed were carefully recorded to correct the measurements to the references values of 15 °C and 15 m/s as in the CFD simulations. The measurements were also corrected by subtracting the drag of the base plate (see Figs. 2 and 4) as well as for blockage using the expressions for solid blockage reported by Barlow et al. (1999). The boundary-layer height was 6 cm, which is below the feet and pedals of the cyclist. The level of turbulence of the approach-flow is lower than 0.2%. The measurement results are reported as mean drag forces together with the simulation results in the next sections.

3. CFD simulations: computational settings and parameters

3.1. Computational geometry and domain

Simulations were performed for separation distances d=0.25, 0.5, 1, 1.5, 2, 2.5, 3.5, 5, 7.5, 10 m. Full-scale and reduced-scale simulations gave identical results, therefore only full-scale simulations are reported in the remainder of this paper. The cyclist and motorcycle are placed in a computational domain with size according to best practice guidelines (Franke et al., 2007, Tominaga et al., 2008) (Fig. 5). The size of the computational domain was $L \times W \times H$=36.1 × 21.2 × 12.4 m^3 for d=1 m. For the other separation distances, the length L of the computational domain was extended accordingly. The maximum blockage ratio was 1.6%, which is well below the recommended maximum value of 3% (Franke et al., 2007, Tominaga et al., 2008). Given this low blockage ratio, the CFD simulations were not corrected for blockage. Note that the distance of the inlet plane to the cyclist was chosen sufficiently large (i.e. 10.2 m) and larger as in the best practice guidelines in order to avoid pressure gradients in/near the inlet plane.

3.2. Computational grid

The grids were based on grid-sensitivity analysis and grid generation guidelines in CFD (Casey and Wintergerste, 2000, Franke et al., 2007, Tominaga et al., 2008) (Fig. 6). A high resolution of cells was used in the boundary-layer region of the cyclist, with the wall-adjacent cell center point at only 30 μm from the body surface. This was needed to allow proper employment of the (scalable) wall functions based on the dimensionless wall unit y^*, which was kept in the range between 4 and 334. The dimensionless wall unit is defined as:

$$y^* = \frac{u^* y_P}{\nu} \quad (2)$$

where u^* is a friction velocity based on the turbulent kinetic energy k_P in the wall-adjacent cell center point P and on the constant C_μ (=0.09):

$$u^* = C_\mu^{1/4} k_P^{1/2} \quad (3)$$

Note that often the parameters y^+ and u^+ are used instead of y^* and u^*. However, the alternatively defined parameters y^* and u^* have the advantage that they allow to specify grid resolution requirements even at locations in the flow field where the shear stress τ_w is zero, which occurs at stagnation and reattachment points, i.e. at the cyclist arms, legs, chest, face and helmet. In that case, y^+ is zero irrespective of the local grid resolution y_P, and cannot be used to specify the grid requirements. The alternative parameter y^*, however, will not be zero because it is based on k_P (Casey and Wintergerste, 2000, Blocken et al., 2009). While 60 μm cells are used at the body surface, further away from the surface, tetrahedral cells were used with an average cell size of about

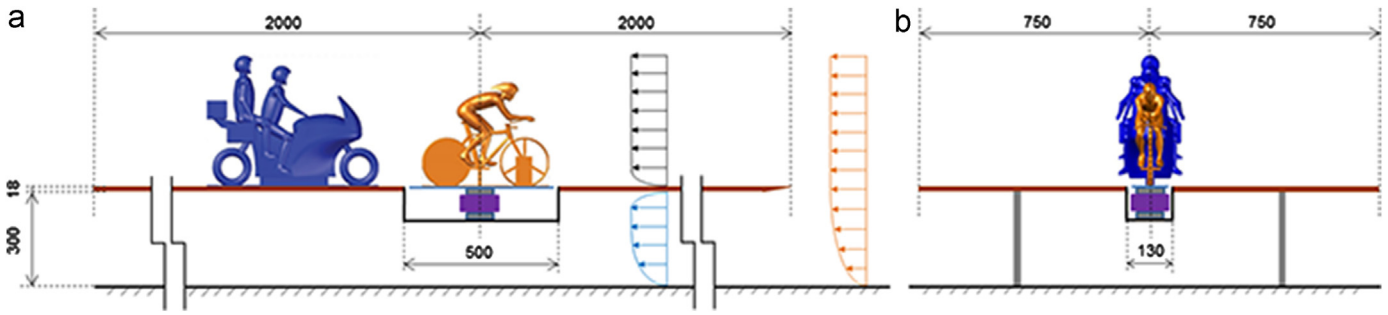

Fig. 3. Wind-tunnel set-up with models on elevated sharp-edged plate to reduce boundary-layer thickness. Dimensions in mm.

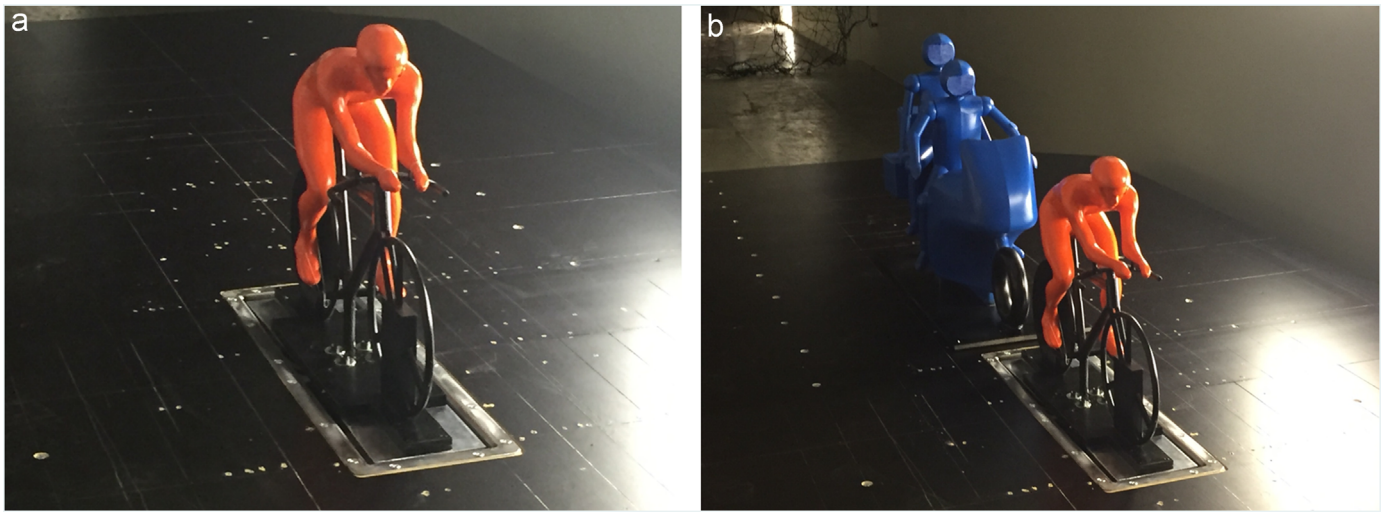

Fig. 4. Photograph of models on elevated plate and embedded force balance in the wind tunnel.

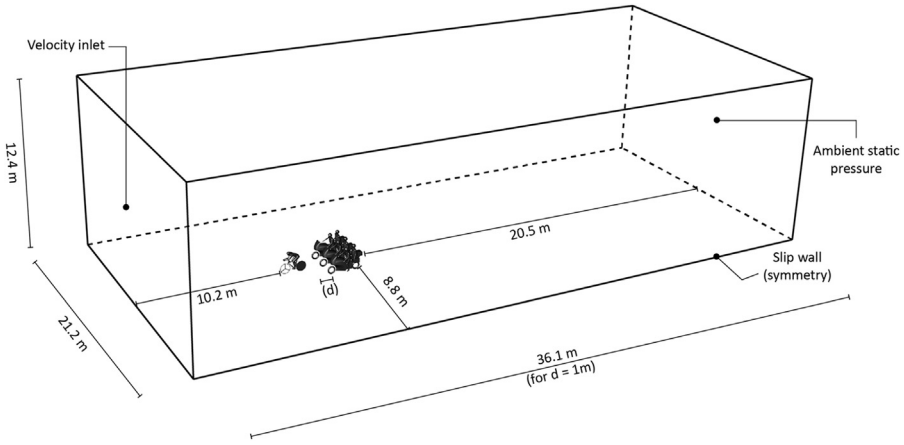

Fig. 5. Computational domain: geometry and some boundary conditions.

0.02 m and hexahedral cells with a cell size of 0.03 m and more. The grid for the motorcycle contained coarser cells, both in the near-wall region as further away, as the cyclist was the focus of the study and highly accurately resolving the near-wall flow near the motorcycle surfaces was deemed unnecessary. The grid for the cyclist subdomain contained about 11×10^6 cells and that for the motorcycle contained about 5×10^6 cells. The total cell count ranged from about 17×10^6 cells for a single following motorcycle at $d = 0.25$ m to about 34×10^6 cells for three following motorcycles at $d = 10$ m. Fig. 6 displays part of the grid in the vertical center plane and on the cyclist and motorcycle surfaces, for the case of three following motorcycles. The figures illustrate the high grid resolution close to the solid body of the cyclist and the lesser grid resolution close to the solid body of the motorcycle.

3.3. Boundary conditions

At the inlet, a uniform velocity of 15 m/s was imposed with a turbulence intensity of 1×10^{-6}%, representing the relative air movement due to cycling at this velocity in still air (zero wind speed). The cyclist and motorcycle body surfaces were modeled as a no-slip walls with zero roughness, at which scalable wall functions were assigned (Grotjans and Menter, 1998). Note that some recent studies on cyclist aerodynamics used low-Reynolds number modeling (LRNM) instead of wall functions (Defraeye et al., 2010a, 2010b, 2011, 2014, Blocken et al., 2013). In the present study however, some parts of the near-wall grid are too coarse for LRNM. For the bottom, side and top boundaries of the domain, a slip-wall boundary (symmetry) was used. Slip walls assume that the normal velocity component and the normal gradients at the boundary are zero, resulting in flow parallel to the boundary. At the outlet of the computational domain, ambient static pressure was imposed.

3.4. Approximate form of governing equations and solver settings

The 3D steady RANS equations were solved with the standard k–ε model (Jones and Launder, 1972) for closure. The choice of the standard k–ε model was made based on previous extensive validation studies for the aerodynamics of a single cyclist, including the standard, realizable and Re-normalization Group (RNG) k–ε model, the standard k–ω model, the Shear-Stress Transport (SST) k–ω model and Large Eddy Simulation. This study, reported in (Defraeye et al., 2010b), showed that the standard k–ε model most accurately predicted the drag, with an underestimation of 4% compared to the corresponding wind-tunnel result. The choice of the standard k–ε model was also based on the earlier study on the aerodynamic benefit of a following car (Blocken and Toparlar, 2015). Pressure-velocity coupling was taken care of by the

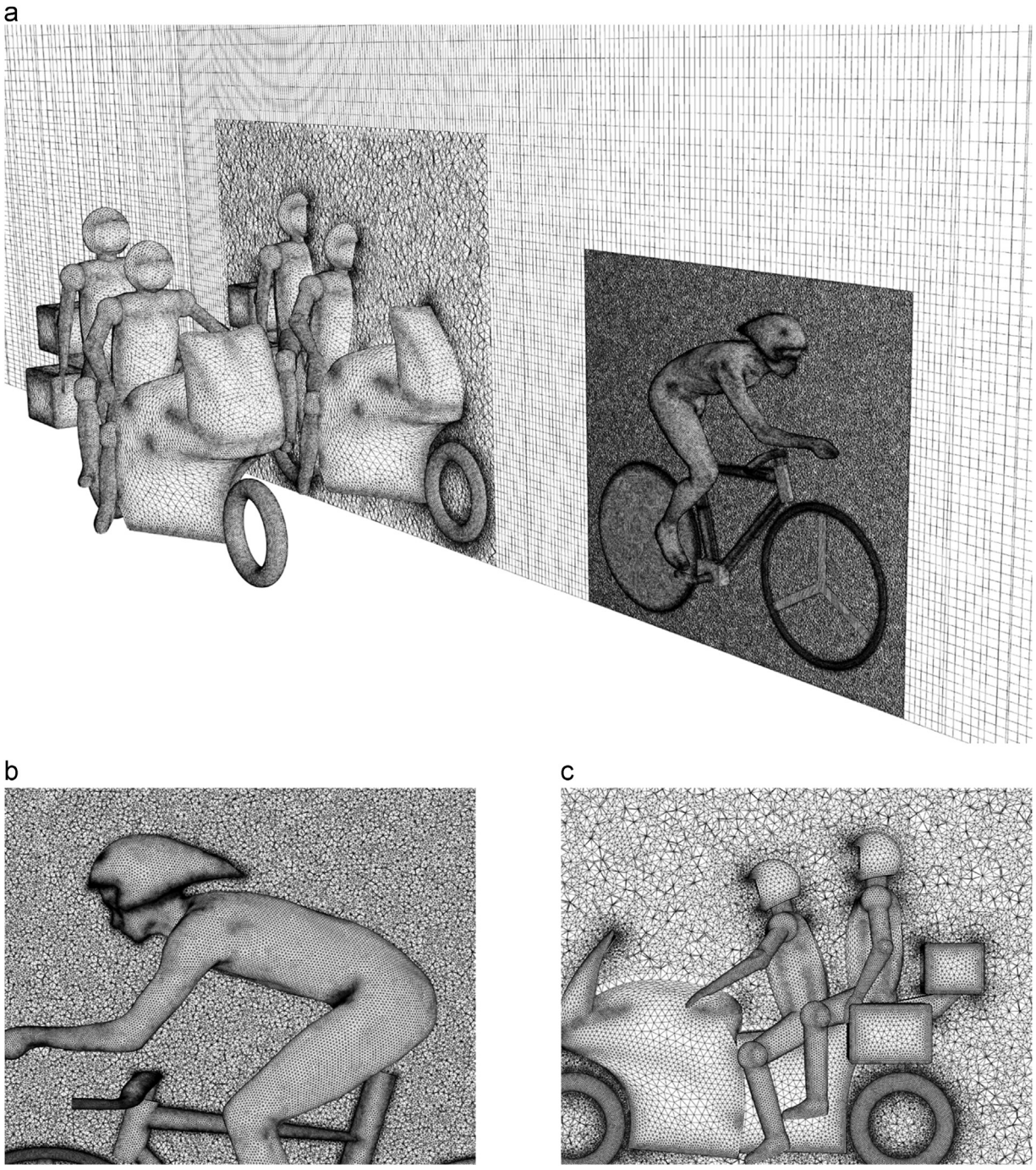

Fig. 6. Computational grid in vertical center plane and on body of cyclist and motorcycle.

SIMPLEC algorithm, pressure interpolation was second order and second-order discretisation schemes were used for both the convection terms and the viscous terms of the governing equations. Gradients are computed with the Green-Gauss cell-based method (ANSYS Fluent, 2013). The simulations were performed with the commercial CFD code ANSYS Fluent 15 (ANSYS Fluent, 2013) which uses the control volume method. Convergence was monitored carefully and the iterations were terminated when all residuals showed no further reduction with increasing number of iterations. At this stage, the scaled residuals were about 10^{-4} for continuity, 10^{-7} for momentum, 10^{-5} for turbulent kinetic energy and 10^{-5} for turbulence dissipation rate.

4. CFD simulations: validation and results

4.1. Validation with wind-tunnel measurements

Fig. 7a displays the CFD results and the wind-tunnel results in terms of the drag of the cyclist (for wind-tunnel results adjusted to full scale), both isolated and in combination with a single trailing motorcycle for $d=0.25$ up to 2.5 m. The errors bars represent the combination of systematic and random errors with 1σ confidence interval. Three observations are made: (i) both CFD simulations and wind-tunnel measurements clearly indicate the reduced cyclist drag due to the presence of the trailing motorcycle and this

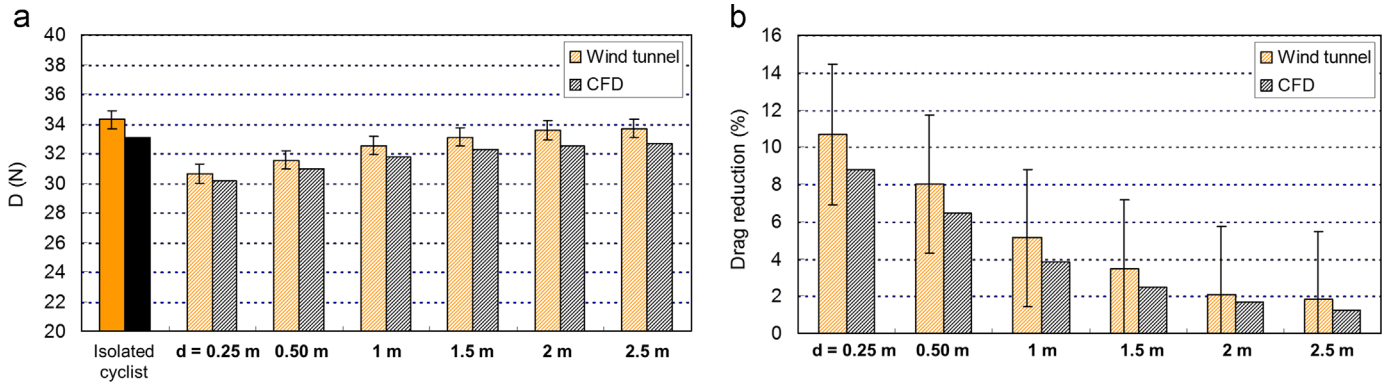

Fig. 7. (a) Drag of isolated cyclist and cyclist followed by single motorcycle as obtained by wind-tunnel tests and CFD simulations. (b) Drag reductions for cyclist followed by single motorcycle by wind-tunnel tests and CFD. Cycling speed is 15 m/s.

effect reduces with increasing distance d; (ii) the CFD simulation results are systematically lower than the wind-tunnel measurements and slightly below the 1σ confidence interval. Test CFD simulations with a no-slip bottom wall and boundary-layer height of 6 cm indicated a negligible influence. Therefore, the underestimation by the CFD simulations is mainly attributed due to the geometric differences between the model geometry in CFD versus wind tunnel. The wind tunnel geometry includes features not present in the CFD model, the most important of which are the vertical reinforcement plates (one for each wheel) and the vertical support column below the crank (Fig. 4). These items provide a larger drag in the wind-tunnel tests than in the CFD simulation. Considering these differences and the confidence intervals as in Fig. 7a, the validation of the CFD simulations is considered to be successful. As the vertical reinforcement plates and support column are not present in reality, the CFD results will be used in the remainder of this paper.

Fig. 7b shows the reduction of the drag of a cyclist followed by a motorcycle compared to an isolated cyclist. The effect is slightly larger in the wind-tunnel measurements than in the CFD simulations. Because the focus is on very small differences between drag values, the errors are significantly amplified. However it is again noted that the errors are based on very conservative estimates and that they include both systematic and random errors, even though the systematic errors were removed by biasing before every measurement series. These statements are corroborated by the clear and monotonically declining trend of the measurement results.

4.2. Drag reduction percentages

Fig. 8 illustrates the drag reduction for the cyclist when followed by one, two or three motorcycles at distances from 0.25 m up to 10 m. While a cyclist closely followed by three motorcycles is less common, a cyclist followed by one motorcycle at the smallest 0.25 m distance is rather common, as evidenced by some of the recent motorcycle-cyclist crashes in Table 1, some of which occurred where cyclists were struck from behind by the motorcycle. The numerical values in Fig. 8 are also given in Table 2. This table also includes the effects by a following car from (Blocken and Toparlar, 2015). For similar distances, logically the drag reduction increases as the number of motorcycles increases, and it is largest for the car, which is the largest following obstacle considered. However, note that the effect of a single following motorcycle at a realistic short distances $d=0.5$ m (6.4%) and $d=1$ m (3.8%) is larger than the effect of a following car at a realistic short distance $d=5$ m (1.4%). As such, it could be argued that in-race motorcycles are not only more dangerous (as evidenced by the many accidents caused by motorcycles as opposed to those caused by cars) but also more influential from the aerodynamic point of view.

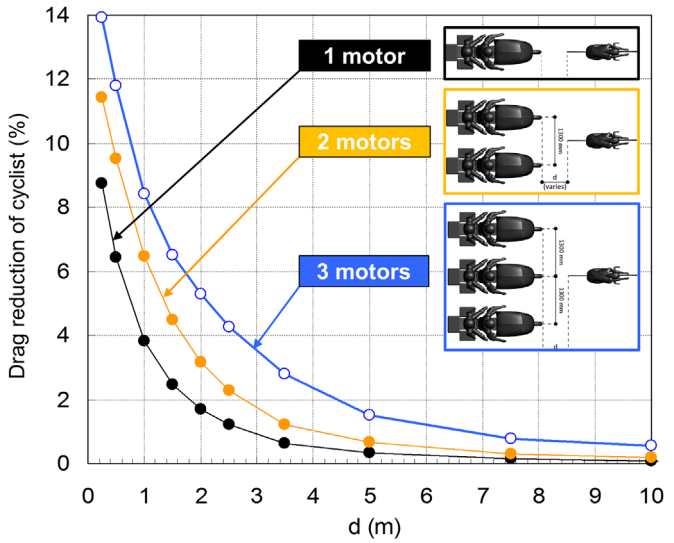

Fig. 8. Drag reduction for cyclist followed by one, two or three motorcycles as a function of the separation distance d. Cycling speed is 15 m/s.

Table 2
Drag reduction (DR) in percent as a function of separation distance d between cyclist and motorcycle(s).

	d (m)									
	0.25	**0.5**	**1**	**1.5**	**2**	**2.5**	**3.5**	**5**	**7.5**	**10**
One motorcycle	8.7	6.4	3.8	2.5	1.7	1.2	0.6	0.3	0.1	0.1
Two motorcycles	11.4	9.5	6.5	4.5	3.2	2.3	1.2	0.7	0.3	0.2
Three motorcycles	13.9	11.8	8.4	6.5	5.3	4.2	2.8	1.5	0.8	0.5
Car			13.7		7.0			1.4		0.2

4.3. Analysis of pressure fields

Fig. 9 shows the pressure coefficient C_p in the vertical center plane for the cyclist and the following motorcycle(s) at six separation distances. Fig. 10 shows the same, but in a horizontal plane at waist height (1.2 m above ground) of the cyclist. The pressure coefficient is defined as:

$$C_P = 2\frac{P-P_0}{\rho U_\infty^2} \quad (4)$$

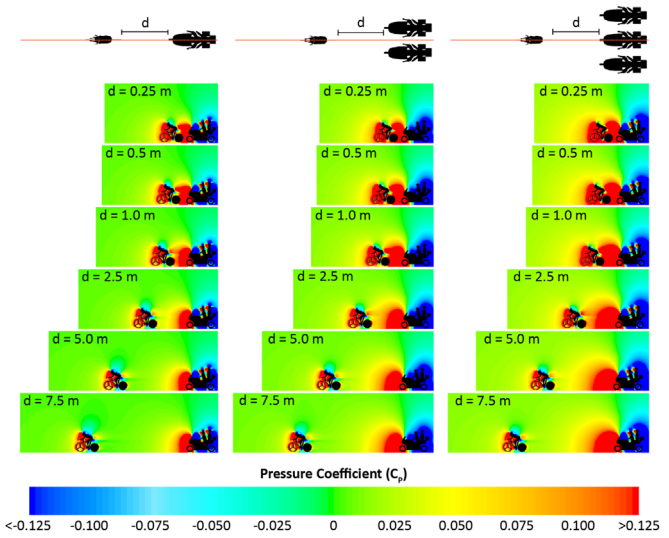

Fig. 9. Pressure coefficient C_P in vertical center plane for cyclist followed by one, two or three motorcycles for separation distances from d=0.25 m up to 7.5 m. Cycling speed is 15 m/s.

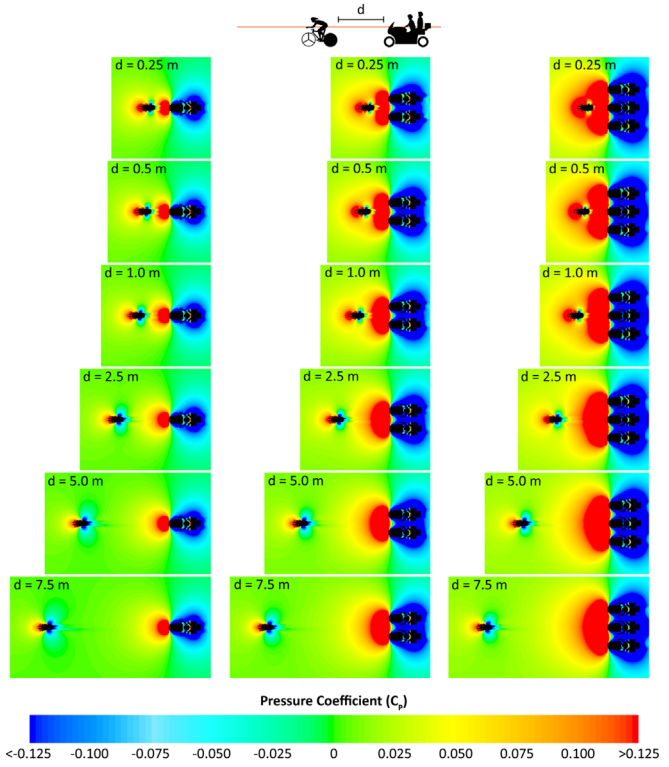

Fig. 10. Pressure coefficient C_P in horizontal plane at height 1.2 above ground for cyclist followed by one, two or three motorcycles for separation distances from d=0.25 m up to 7.5 m. Cycling speed is 15 m/s.

where P is the static pressure and P_0 the reference static pressure (=atmospheric pressure). The legend in Figs. 9 and 10 has been limited to the interval [−0.125; 0.125] to more clearly highlight the changes in the static pressure field. Note that the actual maximum and minimum (absolute) values of C_p are much larger. The figures clearly show the area of overpressure in front of the cyclist and the area of underpressure behind the cyclist. They also show the larger area of overpressure in front of the motorcycle (s) and much larger area of underpressure above and behind the motorcycle(s). When the distance between cyclist and motorcycle (s) decreases, the underpressure area behind the cyclist becomes

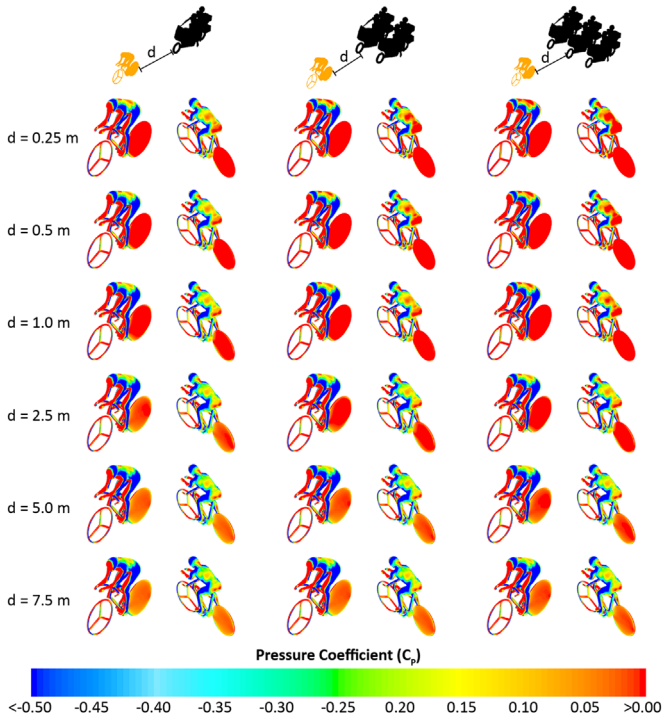

Fig. 11. Pressure coefficient C_P on the body of cyclist and bicycle followed by one, two or three motorcycles for separation distances from d=0.25 m up to 7.5 m. Cycling speed is 15 m/s.

increasingly engulfed by the overpressure area upstream of the motorcycle(s). This causes the underpressure area behind the cyclist not only to decrease or even disappear, it also causes the absolute value of the underpressure on the cyclist and bicycle body to decrease and the absolute value of the overpressure on these bodies to increase, as shown in Fig. 11. Figs. 9 and 10 also show how the motorcycle overpressure and underpressure areas in the case of multiple motorcycles merge to form a single large overpressure and a single large underpressure area, yielding the subsequent larger effects on the cyclist.

5. Potential impact on individual time trials

As in the previous paper (Blocken and Toparlar, 2015), also here nomograms have been developed to assess the potential impact of following motorcycle(s) on the results of an individual time trial. The nomograms are shown in Fig. 12. They provide the time reduction (compared to isolated cyclist case) for a given time trial distance (horizontal axis) assuming that the motorcycle follows the cyclist at a constant distance d throughout the entire individual time trial. For a typical time trial distance of 50 km and for realistic separation distances 0.5 m, 1 m, 2.5 m, 5 m and 10 m, the potential time reduction by exploiting the aerodynamic effect by a single following motorcycle is 108.7 s, 64.2 s, 20.1 s and 5.6 s and 1.0 s, respectively. While these differences can decide whether a cyclist wins or loses an individual time trial, it should be mentioned that it is highly unlikely that a motorcycle will follow the cyclist at this distance for the total duration of the time trial (unless bad intentions would be in play). Therefore, it is more practically relevant to consider benefits obtained over shorter distances within a long time trial. If the motorcycle follows the cyclist for only 1 km (2%) of the 50 km time trial length, the aerodynamic benefits at separation distances 0.25 m, 0.5 m, 1 m, 2.5 m, 5 m and 10 m are 2.98 s, 2.17 s, 1.28 s, 0.40 s, 0.11 s, 0.02 s, which for the shortest distances is still enough to be potentially

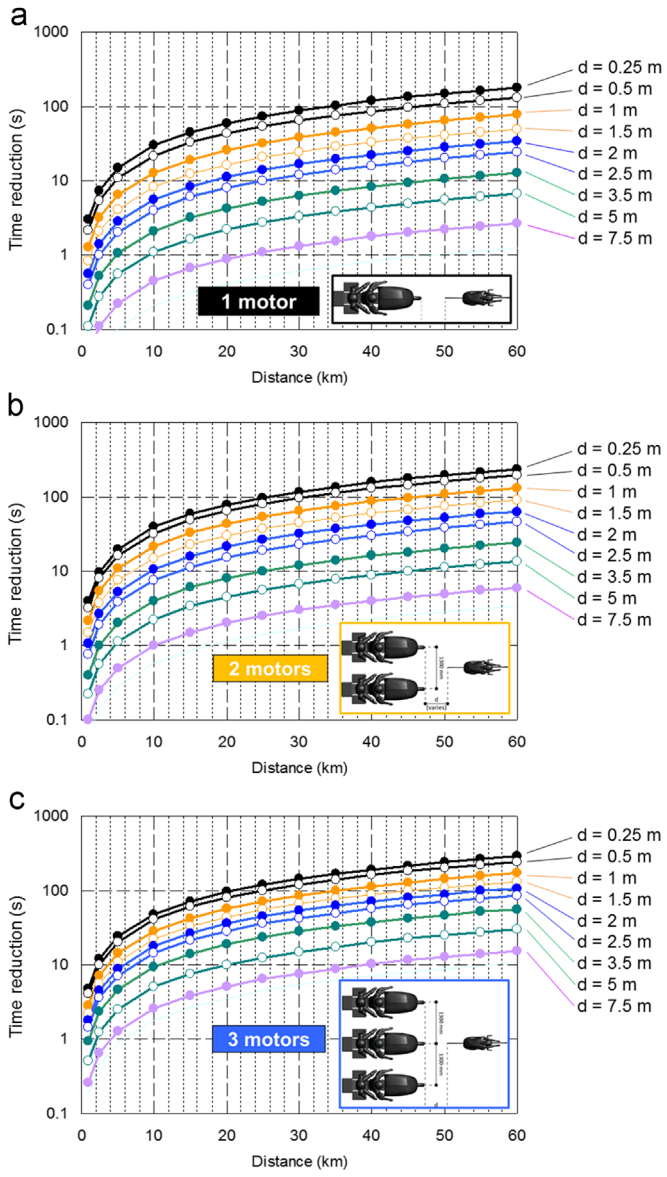

Fig. 12. Nomograms indicating potential time reduction for an individual time trial of given distance for a cyclist when followed by one, two or three motorcycles at separation distance d. Cycling speed is 15 m/s.

decisive. As elite cyclist time trials are often won based on seconds or sometimes even less, these differences can be decisive for who wins the stage. Therefore, it is recommended that the UCI starts to strictly enforce the 10 m minimum distance and even increase it to a larger distance (e.g. 20 or 30 m).

6. Discussion

To the best of our knowledge, the aerodynamic impact of following motorcycle(s) on the drag of a cyclist has not yet been investigated and reported in the scientific literature. The present study is based on a series of CFD simulations validated with wind-tunnel measurements. Both CFD simulations and wind tunnel measurements allowed to ascertain and quantify the substantial drag reduction exerted by following motorcycles on a cyclist. In addition, CFD simulations were also made for the case of two or three following motorcycles. However, the present study also contains some limitations that provide directions for future research. These limitations are similar to those of the earlier study of a cyclist followed by a car (Blocken and Toparlar, 2015).

The bicycle wheels and cyclist legs were stationary, so only static air resistance was considered. Although the largest part of the body is fairly stationary and the present results are considered realistic, future research should focus on analyzing the drag reductions at different pedaling frequencies. The present study only considered a single geometry of cyclist, bicycle and motorcycle. Further research can include cyclists of different height and weight, and with different positions on the bicycle, such as the dropped position during regular road races. Finally, all simulations were performed assuming zero wind speed conditions, i.e. the movement of air was only due to the movement of the cyclist, bicycle and motorcycle in still air. Further studies should investigate the effects of cross wind on the aerodynamic interaction between cyclist and following motorcycle(s).

7. Summary and conclusions

Elite cycling races include three types of vehicles: cyclists, cars and motorcycles. While it is common knowledge that riding behind a car reduces cyclist drag, earlier research (Blocken and Toparlar, 2015) has shown that also a following car can provide a substantial aerodynamic benefit to the cyclist. Extrapolating from these findings, following motorcycles will also provide aerodynamic benefits to the cyclist. The importance of motorcycles in races is exacerbated by many accidents in recent years caused by motorcyclist-cyclist crashes, even yielding fatal injuries as in the Gent-Wevelgem race in Belgium in March 2016. The aerodynamics issues and the accidents have impelled the present authors to perform dedicated wind-tunnel measurements and Computational Fluid Dynamics (CFD) simulations to assess the drag reduction of a cyclist when followed by one, two or three motorcycles. The CFD simulations are performed based on the steady-state Reynolds-Averaged Navier–Stokes equations with the standard k–ε model for closure and are validated by the wind-tunnel tests.

The results indicate that the drag reduction goes up to 8.7% for a single trailing motorcycle and to 13.9% for three trailing motorcycles at a distance of 0.25 m behind the cyclist. Based on a nomogram distilled from the CFD simulations, it was ascertained that for a typical time trial distance of 50 km and for realistic separation distances 0.5 m, 1 m, 2.5 m, 5 m and 10 m, the potential time reduction by exploiting the aerodynamic effect by a single following motorcycle is 108.7 s, 64.2 s, 20.1 s and 5.6 s and 1.0 s, respectively. While these differences can decide whether a cyclist wins or loses an individual time trial, it should be mentioned that it is highly unlikely that a motorcycle will follow the cyclist at this distance for the total duration of the time trial (unless bad intentions would be in play). Therefore, it is more practically relevant to consider benefits obtained over shorter distances within a long time trial. If the motorcycle only follows the cyclist for only 1 km (2%) of the 50 km time trial length, the aerodynamic benefits at separation distances 0.25 m, 0.5 m, 1 m, 2.5 m, 5 m and 10 m are 2.98 s, 2.17 s, 1.28 s, 0.40 s, 0.11 s, 0.02 s, which for the shortest distances is still enough to be potentially decisive.

The effect of a single following motorcycle at a realistic short distances $d=0.25$ m (8.7%), $d=0.5$ m (6.4%) and $d=1$ m (3.8%) is larger than the effect of a following car at a realistic short distance $d=5$ m (1.4%). As such, it could be argued that in-race motorcycles are not only more dangerous (as evidenced by the many cyclist accidents by motorcycles as opposed to those by cars) but also more influential from aerodynamic point of view. As the aerodynamic effects are large enough to make a rider win or lose a time trial, we recommend the International Cycling Union to not

only strictly enforce the minimum distance of 10 m between cyclist and trailing motorcyclists but to set and enforce an even larger one, not only to avoid unwanted aerodynamic benefits, but also to avoid further accidents.

Acknowledgments

This paper is dedicated to the memory of the Belgian rider Antoine Demoitié who died due to a crash with a motorcycle in the international race Gent-Wevelgem in Belgium on 28 March 2016. Our sympathies go out to both the family of the deceased rider but also to the motorcycle rider and his family in the wake of this tragic incident.

The authors thank the technical support team of the Department of the Built Environment at Eindhoven University of Technology: Ing. Jan Diepens, Geert-Jan Maas and Stan van Asten. The authors also thank the anonymous reviewers for their valuable comments.

References

ANSYS Fluent, Release 15.0, Theory Guide, November 2013, ANSYS Inc.

Baker, C.J., 2007. Wind engineering – past, present and future. J. Wind Eng. Ind. Aerodyn. 95 (9-11), 843–870.

Barlow, J.B., Rae, W.H., Pope, A., 1999. Low-speed Wind Tunnel Testing, 3rd Edition Wiley.

Barry, N., Burton, D., Sheridan, J., Thompson, M., Brown, N.A.T., 2015. Aerodynamic drag interactions between cyclists in a team pursuit. Sports Eng. 18 (2), 93–103.

Blocken, B., Defraeye, T., Derome, D., Carmeliet, J., 2009. High-resolution CFD simulations of forced convective heat transfer coefficients at the facade of a low-rise building. Build. Environ. 44 (12), 2396–2412.

Blocken, B., Defraeye, T., Koninckx, E., Carmeliet, J., Hespel, P., 2013. CFD simulations of the aerodynamic drag of two drafting cyclists. Comput. Fluids 71, 435–445.

Blocken, B., 2014. 50 years of computational wind engineering: past, present and future. J. Wind Eng. Ind. Aerodyn. 129, 69–102.

Blocken, B., Toparlar, Y., 2015. A following car influences cyclist drag: CFD simulations and wind tunnel measurements. J. Wind Eng. Ind. Aerodyn. 145, 178–186.

Blocken, B., 2015. Computational fluid dynamics for urban physics: importance, scales, possibilities, limitations and ten tips and tricks towards accurate and reliable simulations. Build. Environ. 91, 219–245.

Broker, J.P., Kyle, C.R., Burke, E.R., 1999. Racing cyclist power requirements in the 4000-m individual and team pursuits. Med Sci Sports Exercise 31 (11), 1677–1685.

Casey, M., Wintergerste, T., 2000. Best Practice Guidelines. ERCOFTAC Special Interest Group on “Quality and Trust in Industrial CFD”, ERCOFTAC.

Defraeye, T., Blocken, B., Koninckx, E., Hespel, P., Carmeliet, J., 2010a. Aerodynamic study of different cyclist positions: CFD analysis and full-scale wind-tunnel tests. J. Biomech. 43 (7), 1262–1268.

Defraeye, T., Blocken, B., Koninckx, E., Hespel, P., Carmeliet, J., 2010b. Computational Fluid Dynamics analysis of cyclist aerodynamics: Performance of different turbulence-modelling and boundary-layer modelling approaches. J. Biomech. 43 (12), 2281–2287.

Defraeye, T., Blocken, B., Koninckx, E., Hespel, P., Carmeliet, J., 2011. Computational fluid dynamics analysis of drag and convective heat transfer of individual body segments for different cyclist positions. J. Biomech. 44 (9), 1695–1701.

Defraeye, T., Blocken, B., Koninckx, E., Hespel, P., Verboven, P., Nicolai, B., Carmeliet, J., 2014. Cyclist drag in team pursuit: influence of cyclist sequence, stature, and arm spacing. J. Biomech. Eng. – ASME 136 (1), art. no. 011005.

Edwards, A.G., Byrnes, W.C., 2007. Aerodynamic characteristics as determinants of the drafting effect in cycling. Med. Sci. Sports Exerc. 39 (1), 170–176.

Fintelman, D.M., Hemida, H., Sterling, M., Li, F.X., 2015. CFD simulations of the flow around a cyclist subjected to crosswinds. J. Wind Eng. Aerodyn. 144, 31–41.

Franke, J., Hellsten, A., Schlünzen, H., Carissimo, B., 2007. Best practice guideline for the CFD simulation of flows in the urban environment, COST Action 732: Quality Assurance and Improvement of Microscale Meteorological Models, Hamburg, Germany.

Gore, M., 2016. Personal Communication with Sensor Manufacturer..

Grappe, G., Candau, R., Belli, A., Rouillon, J.D., 1997. Aerodynamic drag in field cycling with special reference to the Obree's position. Ergonomics 40 (12), 1299–1311.

Grotjans, H., Menter, F., 1998. Wall functions for general application CFD codes, in: Proceedings of the 4th Computational Fluid Dynamics Conference (ECCOMAS '98), John Wiley & Sons, pp. 1112–1117.

Hagberg, J.M., McCole, S.D., 1990. The effect of drafting and aerodynamic equipment on the energy expenditure during cycling. Cycl. Sci. 2 (3), 19–22.

Hanna, R.K., 2002. Can CFD make a performance difference in sport? In: Ujihashi, S., Haake, S.J. (Eds.), The Engineering of Sport 4. Blackwell Science, Oxford, pp. 17–30.

Iniguez-de-la-Torre, A., Iniguez, J., 2009. Aerodynamics of a cycling team in a time trial: does the cyclist at the front benefit? Eur. J. Phys. 30, 1365–1369.

International Cycling Union, 2013. Footage of 2013 UCI Road World Championships in Toscany, Italy. ⟨https://www.youtube.com/watch?v=cNboQxBChfc⟩.

International Cycling Union, 2014. Footage of 2014 UCI Road World Championships in Ponferrada, Spain. ⟨https://www.youtube.com/watch?v=nW8aiTx0ARg⟩.

International Cycling Union 2015a. Footage of 2015 UCI Road World Championships in Richmond, USA. ⟨https://www.youtube.com/watch?v=ETT7vptNW7I⟩.

International Cycling Union, 2015b. UCI Cycling Regulations, Part 2, Road Races, Version 05.02.2015.

International Cycling Union 2016. UCI Cycling Regulations, Part 2, Road Races, Version 01.03.2016.

Jones, W.P., Launder, B.E., 1972. The prediction of laminarization with a two-equation model of turbulence. Int. J. Heat Mass Transf. 15, 301–314.

Kyle, C.R., Burke, E.R., 1984. Improving the racing bicycle. Mech. Eng. 106 (9), 34–45.

Kyle, C.R., 1979. Reduction of wind resistance and power output of racing cyclists and runnings travelling in groups. Ergonomics 22 (4), 387–397.

Lukes, R.A., Chin, S.B., Haake, S.J., 2005. The understanding and development of cycling aerodynamics. Sports Eng. 8, 59–74.

Lukes, R.A., Hart, J.H., Chin, S.B., Haake, S.J., 2004. The aerodynamics of mountain bicycles: the role of computational fluid dynamics. In: Hubbard, M., Mehta, R.D., Pallis, J.M. (Eds.), The Engineering of Sport 5. International Sports Eng. Association, Sheffield.

Meroney, R.N., Derickson, R., 2014. Virtual reality in wind engineering: the windy world within the computer. J. Wind Eng. 11 (2), 11–26.

Meroney, R.N., 2016. Ten questions concerning hybrid computational/physical model simulation of wind flow in the built environment. Build. Environ. 96, 12–21.

McCole, S.D., Claney, K., Conte, J.-C., Anderson, R., Hagberg, J.M., 1990. Energy expenditure during bicycling. J. Appl. Physiol. 68 (2), 748–753.

Murakami, S., 1997. Current status and future trends in computational wind engineering. J. Wind Eng. Ind. Aerodyn. 67–68, 3–34.

Olds, T., 1998. The mathematics of breaking away and chasing in cycling. Eur. J. Appl. Physiol. 77, 492–497.

Solari, G., 2007. The International Association for Wind Engineering (IAWE): progress and prospects. J. Wind Eng. Ind. Aerodyn. 95, 813–842.

Stathopoulos, T., 1997. Computational wind engineering: past achievements and future challenges. J. Wind Eng. Ind. Aerodyn. 67–68, 509–532.

Tominaga, Y., Mochida, A., Yoshie, R., Kataoka, H., Nozu, T., Yoshikawa, M., Shirasawa, T., 2008. AIJ guidelines for practical applications of CFD to pedestrian wind environment around buildings. J. Wind Eng. Ind. Aerodyn. 96 (10–11), 1749–1761.

Wilson, D.G., 2004. Bicycling Science, Third Edition MIT Press, Cambridge, MA.

Zdravkovich, M.M., Ashcroft, M.W., Chisholm, S.J., Hicks, N., 1996. Effect of cyclist's posture and vicinity of another cyclist on aerodynamic drag. In: Haake (Ed.), The Engineering of Sport. Balkema, Rotterdam, pp. 21–28.